Should I tilt or should I push? Effect of contact force and catheter inclination in cardiac radiofrequency ablation

Massimiliano Leoni[1], Argyrios Petras[1], Zoraida Moreno Weidmann[2], Jose M Guerra[2], Luca Gerardo-Giorda[1,3]

[1] Johann Radon Institute for Computational and Applied Mathematics (RICAM), Austrian Academy of Sciences, Linz, Austria
[2] Department of Cardiology, Hospital de la Santa Creu i Sant Pau, IIB Sant Pau, Universitat Autònoma de Barcelona, CIBER CV, Barcelona, Spain
[3] Institute for Mathematical Methods in Medicine and Data-Based Modelling, Johannes Kepler University, Linz, Austria

Abstract

Radiofrequency ablation is a minimally invasive treatment for cardiac arrhythmias. During the procedure, the catheter is placed at the arrhythmogenic site to deliver electric current. There is uncertainty in the contact force and the catheter orientation, which can be affected by many factors, including the cardiac anatomy and the heartbeat. In this work we explore the impact of the contact force and different catheter inclinations on the resulting lesion. An improved electrical model allows to properly account for the current that flows to the tissue through the blood, a relevant aspect when the catheter is not perpendicular. The lesion size consistently increases with the catheter inclination, regardless of the contact force.

1. Introduction

Radiofrequency ablation is a standard, minimally invasive, treatment for several cardiac arrhythmias. The catheter is placed on the arrhythmogenic tissue delivering electrical current at frequencies of 450–500 kHz to produce thermal lesions. The contact surface between the catheter tip and the cardiac wall (electrode footprint) is a major determinant of the amount of power dissipated into the tissue, but it is not the only one. Increasing the contact force increases the footprint but, if the electrode is placed vertically on the tissue, a large amount of power is dissipated in the blood. On the other hand, when the catheter is tilted, part of the current flowing through the electrode-blood interface actually passes to the tissue (see Figure 1), thus increasing the power delivered to the latter.

In this study we explore the impact of catheter orientation and contact force on the resulting lesion size. We
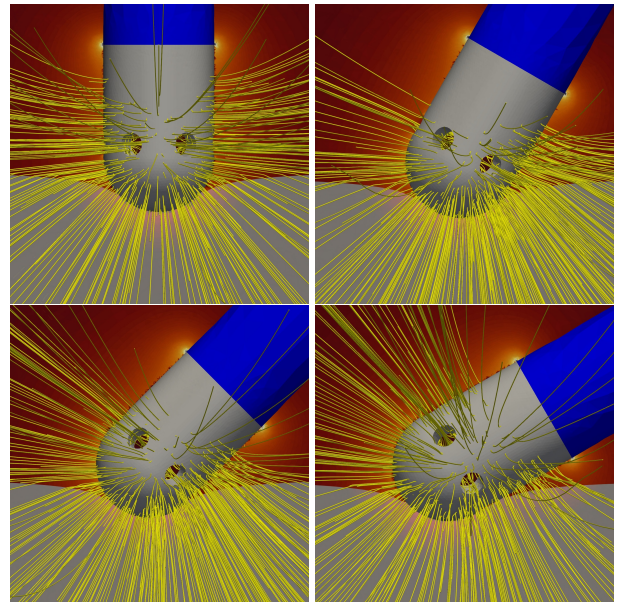

Figure 1. The electric field at $10\,\mathrm{g}$ of contact force and different orientation angles (from top left to bottom right: $0°$, $30°$, $45°$ and $60°$).

introduce an upgraded version of the model in [1] which accounts for the material properties of the cardiac wall and for the current that flows to the tissue, both from direct contact with the electrode and through the blood.

2. Methods

2.1. Geometry

The computational domain Ω, mimicking an in-vitro experimental setup for a porcine ventricle [2], is a cylin-

der of radius $40\,\mathrm{mm}$ and height $80\,\mathrm{mm}$, where blood Ω_b ($40\,\mathrm{mm}$), tissue Ω_t ($20\,\mathrm{mm}$) and a polymethyl methacrylate board ($20\,\mathrm{mm}$) are layered. The tissue slab contains fibers pointing along the x-axis. A catheter is submerged in the blood, featuring a hemispherical tip electrode of diameter 7 Fr, 6 pores connected to a common irrigation channel in the center of the electrode, and a thermistor, as in [1].
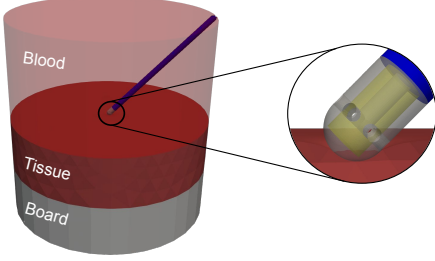

Figure 2. The computational domain.

2.2. Mathematical model

The mechanical interaction of the electrode tip with the tissue is assumed to be a frictionless contact and follows the mechanical equilibrium equation, solved only on the tissue subdomain. The blood flow and its interaction with the irrigated saline are modelled using the incompressible Navier-Stokes equations, which are solved only in the blood subdomain. A modified Penne's bioheat equation models the temperature changes in the system, with an advection cooling term and an electric heat source. The electrical potential follows a quasi-static elliptic equation along with a power constraint equation and is solved along with the bioheat equation in the entire domain. The full system in the current configuration reads as follows:

$$\operatorname{div}\Sigma = \mathbf{0}$$
$$\frac{\partial \mathbf{v}}{\partial t} + \mathbf{v}\cdot\nabla\mathbf{v} - \operatorname{div}\tau(\mathbf{v},p) = \mathbf{0}, \qquad \operatorname{div}\mathbf{v} = 0,$$
$$\rho(T)c(T)\left(\frac{\partial T}{\partial t} + \mathbf{v}\cdot\nabla T\right) - \operatorname{div}(k(T)\nabla T) = \sigma(T)|\nabla\Phi|^2, \quad (1)$$
$$\operatorname{div}(\sigma(T)\nabla\Phi) = 0,$$
$$\int_\Omega \sigma(T)|\nabla\Phi|^2 \,\mathrm{d}x + R\int_{\Gamma_{out}} (\sigma(T)\nabla\Phi\cdot\mathbf{n})^2 \,\mathrm{d}s = P.$$

In (1), Σ is the Cauchy stress tensor, $\mathbf{v}$ is the velocity, t is the time, τ is the stress tensor, p is the pressure scaled by the density, ρ is the density, c is the specific heat, T is the temperature, k and σ are the (temperature-dependent) thermal and electrical conductivities, Φ is the electrical potential, Ω is the computational domain, Γ_{out} is the portion of the domain boundary that separates the blood and the tissue from the outside (id est, $\Gamma_{out} = \partial\Omega\cap(\partial\Omega_t\cup\partial\Omega_b)$), R is the resistance offered by everything that is outside the

domain and P is the power setting from the ablation protocol. More details on the model can be found in [1].

The cardiac muscle is a hyperelastic, nearly-incompressible orthotropic material which is modelled using the strain energy function presented in [3]

$$\Psi = C(e^Q - 1) + \kappa(\ln J)^2,$$
$$Q = b_{ff}\overline{E}_{ff}^2 + b_{ss}\overline{E}_{ss}^2 + b_{nn}\overline{E}_{nn}^2 \qquad (2)$$
$$+ 2(b_{fs}\overline{E}_{fs}^2 + b_{sn}\overline{E}_{sn}^2 + b_{fn}\overline{E}_{fn}^2),$$

where C is the material constant, κ is the bulk modulus, J is the volume ratio and $\overline{\mathbf{E}}$ and $\mathbf{b}$ are the isochoric Green-Lagrange strain tensor and the anisotropic stiffness coefficients in the axial and shear direction respectively (f: fiber, s: sheet and n: normal).

We solve system (1) with a self-developed code that uses the finite element method, implemented on the FEniCSx computing platform (`fenicsproject.org`). The simulations were run on the in-house HPC cluster of RICAM.

2.3. Boundary conditions

We impose the Signorini-Hertz-Moreau frictionless contact boundary conditions on the tissue's upper surface, written as

$$\Sigma_n < 0, \quad g \ge 0, \quad \Sigma_n g = 0, \quad \Sigma_t = \mathbf{0},$$

where $\Sigma_n = \Sigma\cdot\mathbf{n}\cdot\mathbf{n}$, $\Sigma_t = \Sigma\cdot\mathbf{n} - \Sigma_n\mathbf{n}$ and g is the selected gap function. The tissue is fixed at the bottom and all the remaining boundaries are equipped with homogenous Neumann boundary conditions.

We impose an inflow $\mathbf{v}_b = (v_x, 0, 0)$ on the boundary of the blood chamber that satisfies $\mathbf{v}_b \cdot \mathbf{n} \le 0$ and an outflow zero-pressure condition on the opposite side. The saline inflow is a parabolic velocity profile with a flux of $17\,\mathrm{mL/min}$ at the top boundary of the irrigation channel. We apply no-slip conditions on all the remaining boundaries.

At the top surface of the electrode we set a potential ensuring that the system satisfies the constant-power constraint and a resistance of $R_{sys} = 121\,\Omega$. A zero-voltage condition is set at the bottom of the methacrylate board. No-flux boundary conditions are applied on the sides of the board and on the catheter shaft, while we impose Robin boundary conditions on the top and lateral sides of the blood boundary as well as on the lateral tissue boundary

$$-\sigma(T)\nabla\Phi\cdot\mathbf{n} = \frac{\Phi}{R}.$$

The saline flows in at $28\,^\circ\mathrm{C}$ [4] and no-thermal-flux conditions are imposed on the surface of the catheter shaft. The remaining boundaries of the computational domain are at a constant body temperature of $37\,^\circ\mathrm{C}$.

2.4. Model parameters

Our model includes a porcine cardiac tissue slab submerged in porcine blood. The model parameters are drawn from the literature [1, 3, 5–8]. Table 1 summarizes the values of the density ρ in $\mathrm{kg/m^3}$, the specific heat c in $\mathrm{J\,kg^{-1}\,K^{-1}}$, the electrical conductivity σ in $\mathrm{S/m}$ and the thermal conductivity k in $\mathrm{W\,m^{-1}\,K^{-1}}$ for the different subdomains of the model.

Table 1. The biophysical parameters of the model.

	Blood	Tissue	Board	Electrode	Thermistor
ρ	1020	$\rho(T)$	1185	21500	32
c	3454	$c(T)$	1466	132	835
σ	$\sigma_b(T)$	$\sigma_t(T)$	10^{-10}	4.6×10^6	10^{-5}
k	0.3	$k(T)$	0.209	71	0.038

The tissue specific heat and thermal conductivity depend on the temperature exponentially while the tissue and blood electrical conductivity do so linearly:

$$\rho(T)c(T) = \left(3.643 - 0.003533e^{0.06263T}\right) \times 10^6,$$
$$k(T) = 0.5655 + 5.034 \times 10^{-12}e^{0.263T},$$
$$\sigma_t(T) = 0.54\left(1 + 0.015(T - T_b)\right),$$
$$\sigma_b(T) = 1.2\left(1 + 0.011(T - T_b)\right),$$

where $T_b = 37\,^\circ\mathrm{C}$ is the body temperature.

We tune the passive material stiffness to match the tissue-electrode contact area and the contact force at $10\,\mathrm{g}$ in [1]. The identified value is $C = 10.3\,\mathrm{kPa}$.

Finally, the resistance R is tuned to match the power $P = 30\,\mathrm{W}$ and the resistance $R_{sys} = 121\,\Omega$ at $10\,\mathrm{g}$ and is kept constant for all different simulated scenarios.

2.5. Lesion estimation

We use a three-state cell-death model calibrated for cardiomyocytes [9] to identify the resulting lesion. The measured dimensions are the lesion volume (V), maximum width (W) and depth (D), as measured from the undeformed tissue surface.

2.6. Ablation protocol

We simulate a standard protocol of $30\,\mathrm{W}$ for $30\,\mathrm{s}$, followed by a long thermal relaxation (see [9] for details). We consider two different contact force profiles, $10\,\mathrm{g}$ and $20\,\mathrm{g}$, and different orientation angles, starting from perpendicular orientation (0°) and tilting the catheter by 30°, 45° and 60° from the vertical axis. The saline irrigation rate is set to $17\,\mathrm{mL/min}$ during the ablation, to the standby mode of $2\,\mathrm{mL/min}$ during the first $30\,\mathrm{s}$ of thermal relaxation and to zero afterwards. The blood velocity is $0.5\,\mathrm{m/s}$ as in [1].

3. Results

Table 2 collects lesion width, depth and volume for all inclinations and contact forces.

As already observed for a perpendicular electrode in our previous work [10], the contact force has a significant impact on the lesion size for all tilting angles.

Catheter orientation does not seem to significantly affect the lesion depth, but it has a clear impact on width and volume. Both are consistently increasing as the inclination angle increases, with 60° having a larger lesion volume by $29\,\%$ for $10\,\mathrm{g}$ and $39\,\%$ in the case of $20\,\mathrm{g}$.

Table 2. Depth from the undeformed surface (D in mm), width (W in mm) and volume (V in $\mathrm{mm^3}$) of the lesion for different contact forces and inclination angles.

Force / Angle	10 g			20 g		
	D	W	V	D	W	V
0°	4.86	7.26	130.6	5.46	7.94	168.5
30°	4.90	7.33	131.8	5.48	8.11	176.4
45°	4.96	7.63	145.0	5.57	8.48	199.9
60°	5.11	8.14	169.0	5.75	9.02	233.5

Figure 3 shows the resulting lesions for all the considered contact forces and inclinations. Observe that the irreversible surface lesion becomes larger as the catheter angle increases, with the largest ones at 60°. In terms of shape, more skewed lesions are obtained for higher catheter inclinations.

It is worth noticing that tilting the catheter to 60° with a contact force of $10\,\mathrm{g}$ produces a lesion comparable in volume to a perpendicular catheter with $20\,\mathrm{g}$. However, the resulting lesion shape is much different, since the lesion is $0.35\,\mathrm{mm}$ shallower and $0.2\,\mathrm{mm}$ wider.

4. Conclusions

The catheter inclination plays an important role in determining the lesion size and shape. For thin tissues like that of the atrium, a large inclination might be the preferred approach to achieve a wider lesion to completely eliminate the arrhythmogenic substrate with fewer point-by-point ablations. On the other hand, the contact force plays a dominant role on the lesion depth, which might be necessary to achieve transmurality in thicker tissues like the ventricle.
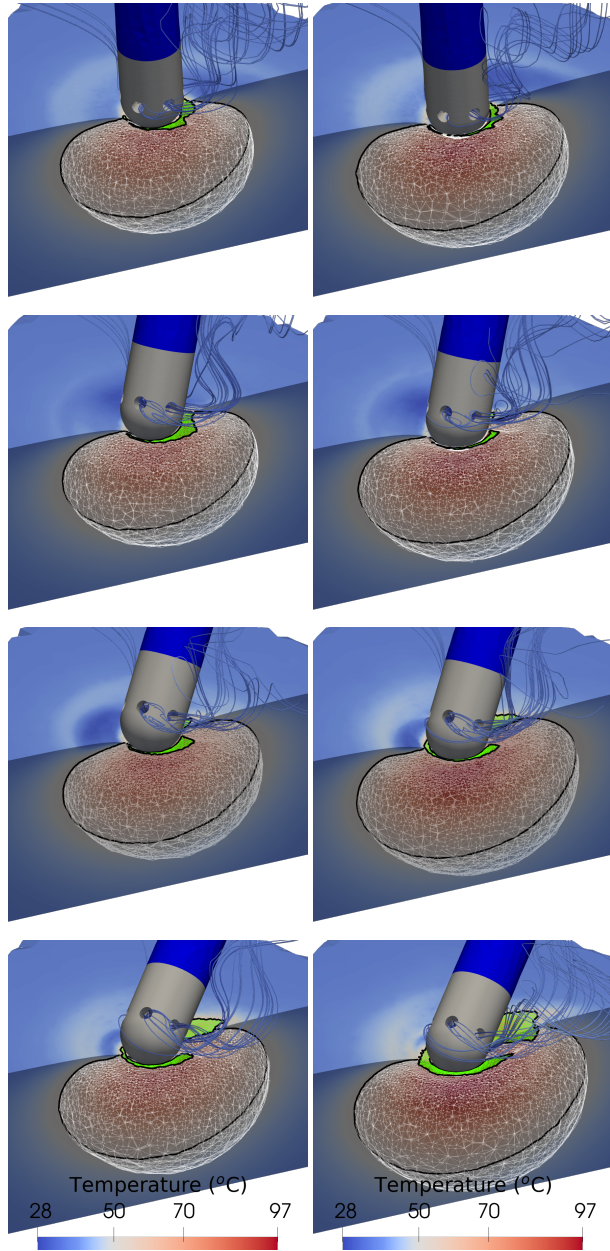
Figure 3. Temperature distribution after $30\,\mathrm{s}$ of ablation for $10\,\mathrm{g}$ (left column) and $20\,\mathrm{g}$ (right) and different orientation angles (from top to bottom: $0°$, $30°$, $45°$ and $60°$). The lesion identified by the three-state model is shown in white, the irreversible superficial damage in green. The irrigation saline streamlines are shown in blue.

Acknowledgments

References

[1] Petras A, Leoni M, Guerra JM, Jansson J, Gerardo-Giorda L. A computational model of open-irrigated radiofrequency catheter ablation accounting for mechanical properties of the cardiac tissue. International Journal for Numerical Methods in Biomedical Engineering 2019;35(11):e3232.

[2] Guerra JM, Jorge E, Raga S, Gálvez-Montón C, Alonso-Martín C, Rodríguez-Font E, Cinca J, Viñolas X. Effects of open-irrigated radiofrequency ablation catheter design on lesion formation and complications: in vitro comparison of 6 different devices. Journal of Cardiovascular Electrophysiology 2013;24(10):1157–1162.

[3] Usyk TP, Mazhari R, McCulloch AD. Effect of laminar orthotropic myofiber architecture on regional stress and strain in the canine left ventricle. Journal of Elasticity 2000; 61:143–164. ISSN 03743535.

[4] Squara F, Maeda S, Aldhoon B, Marginiere J, Santangeli P, Chik WW, Michele J, Zado E, Marchlinski FE. In vitro evaluation of ice-cold saline irrigation during catheter radiofrequency ablation. Journal of Cardiovascular Electrophysiology 2014;25(10):1125–1132.

[5] Bianchi L, Bontempi M, De Simone S, Franceschet M, Saccomandi P. Temperature dependence of thermal properties of ex vivo porcine heart and lung in hyperthermia and ablative temperature ranges. Annals of Biomedical Engineering 2023;1–18.

[6] Wen J, Wan N, Bao H, Li J. Quantitative measurement and evaluation of red blood cell aggregation in normal blood based on a modified hanai equation. Sensors 2019; 19(5):1095.

[7] Jaspard F, Nadi M. Dielectric properties of blood: an investigation of temperature dependence. Physiological measurement 2002;23(3):547.

[8] Rosentrater KA, Flores RA. Physical and rheological properties of slaughterhouse swine blood and blood components. Transactions of the ASAE 1997;40(3):683–689.

[9] Petras A, Leoni M, Guerra JM, Gerardo-Giorda L. Calibration of a three-state cell death model for cardiomyocytes and its application in radiofrequency ablation. Physiological Measurement 2023;44(6):065003.

[10] Petras A, Weidmann ZM, Ferrero ME, Leoni M, Guerra JM, Gerardo-Giorda L. Impact of electrode tip shape on catheter performance in cardiac radiofrequency ablation. Heart Rhythm O2 2022;3(6):699–705.

Address for correspondence:

Massimiliano Leoni
RICAM
Altenbergerstrasse 69, 4040 Linz, Austria
massimiliano.leoni@ricam.oeaw.ac.at